Journal of Sound and Vibration (2002) **254**(1), 105–116
doi:10.1006/jsvi.2001.4087, available online at http://www.idealibrary.com on IDEAL®

TIME–FREQUENCY ANALYSIS OF A SUSPENSION BRIDGE BASED ON GPS

L. Xu, J. J. Guo and J. J. Jiang

Department of Civil Engineering, RM 610 *Bldg.* 20, *Tsinghua University, Beijing* 100084, *People's Republic of China. E-mail: xuliang99@mails.tsinghua.edu.cn*

(*Received* 23 *March* 2001, *and in final form* 4 *September* 2001)

This paper describes the results obtained from full-scale measurements of Humen bridge, which is the second longest suspension bridge in China. A real-time kinematic (RTK) global positioning system (GPS) has been developed and installed on the Humen bridge for on-line monitoring of bridge deck movements. The field wind-induced vibration data were measured by this monitoring system. Three system identification techniques are then adopted in the modal analysis of the wind-induced vibration response: the time–frequency Wigner distribution (WD) technique, the frequency-domain fast Fourier transform (FFT) technique and the time-domain auto-regressive moving average vector (ARMAV) technique. The WD technique can recognize close modal coupling and non-stationary response. The FFT technique can on site verify the quality of the measurements, but its frequency resolution is low and damping estimates are unreliable. The ARMAV method allows for gaining high-frequency resolution. However, it is strictly related to the stationary hypothesis. It is a general conclusion that we can improve the quality of the analysis and get more precise characteristics of the signal by these three methods. In addition, the WD combined with ARMAV seems to be the best case in quantitative analysis of fast-changing vibration signals.

1. INTRODUCTION

The aim of the system identification is to determine the structural modal parameters from dynamic measurements, which are very useful in model update, damage assessment, active control and original design reevaluation.

There are some ambient or natural excitations, such as traffic, wind, earthquake and their combination. Then it is very attractive to apply the system identification techniques to ambient vibration measurements. Because in this case, only response data of ambient vibrations are measurable and the actual loading conditions are still unknown. At present, there are several system identification techniques using only the output signal.

Ibrahim [1] developed the Ibrahim time domain (ITD) identification technique, which was able to identify the vibration modes from the free vibration response. In order to extract modes from ambient vibration data, Cole [2, 3] introduced the random decrement (RD) technique to achieve free vibration data from ambient vibration data. And Huang [4] field-tested the Yuan-Shan bridge and validated this technique.

The other technique is the auto-regressive moving average vector (ARMAV); it was used to analyze the time series obtained from the output signal [5, 6]. Now this technique can be applied to the modal identification of the environment-excited real bridges, which has been proved by Garibaldi [7].

0022-460X/02/$35.00

The most advanced method for ambient vibration measurement may be the stochastic subspace identification (SSI) technique, proposed by Peeters [8]. This time domain identification method can extract structural modal parameters based on the state-space model, avoiding the influence of conventional manual identification and iterative process.

However, it is well known that wind speed and wind-induced vibration can be reasonably modelled as non-stationary random processes [9]. General system identification techniques, including all the above methods, are still inadequate for the detection of local transient signal characteristics. This paper will address time–frequency WD technique to study the non-stationary wind-induced vibration response of suspension bridge. The results obtained by this method will be compared with those by traditional FFT and ARMAV methods.

2. WIGNER DISTRIBUTION

Wigner distribution (WD) was originally applied in quantum physics [10]. Ville firstly used this technique on harmonic analysis [10] and the result carries the implications of the instantaneous power and instantaneous frequency [11]. Later, Bonato identified modal frequencies and local equivalent viscous damping of pylon with this technique [12].

The time–frequency distribution of signal $s(u)$ may be expressed in the following form:

$$w(t, \omega) = \frac{1}{2\pi} \int_{-\infty}^{\infty} \int_{-\infty}^{\infty} \int_{-\infty}^{\infty} s\left(u + \frac{\tau}{2}\right) s^*\left(u - \frac{\tau}{2}\right) g(\theta, \tau) \mathrm{e}^{-\mathrm{j}(\theta t + \omega\tau - \omega\theta)} \, \mathrm{d}\theta \, \mathrm{d}u \, \mathrm{d}\tau, \tag{1}$$

where $w(t, \omega)$ is the time–frequency distributions, $s(u)$ is the signal under consideration, $s^*(u)$ is the complex conjugate of the signal, t is the time, f is the frequency, τ is the time lag, θ is the frequency lag, and $g(\theta, \tau)$ is referred to as the kernel of the transform. We always consider $s(u)$ as the analytic signal obtained from the real recording. Equation (1) leads to the definition of four different domains: the temporal correlation (u, τ), the spectral correlation (θ, f), the ambiguity (θ, τ), and the time–frequency (u, f).

The most popular transform is the Wigner–Ville transform that can be derived from the general formula given in equation (1) with $g(\theta, \tau) = 1$. The Wigner–Ville transform is generally satisfactory when applied to deterministic signals constituted by a single-frequency component. On the contrary, it is not well suited for being applied to multi-frequency component signals, since the bilinearity of the transform induces the presence of interference terms [13]. These interference terms may not be easily distinguished from authentic signal components, thus making it difficult the interpretation of distributions obtained from multi-component signals.

In order to eliminate the cross-term interference, Choi and Williams [14] introduced the exponential kernel in equation (1) given by

$$g(\theta, \tau) = \mathrm{e}^{-\theta^2\tau^2/\sigma}, \tag{2}$$

where σ is the attenuate coefficient. The kernel is defined in the θ, τ plane, which is referred to as ambiguity plane. In this domain, the kernel of the transform is multiplied by the ambiguity function, thus obtaining the characteristic function

$$M(\theta, \tau) = g(\theta, \tau) A(\theta, \tau), \quad \text{where } A(\theta, \tau) = \int_{-\infty}^{\infty} s\left(t + \frac{\tau}{2}\right) s^*\left(t - \frac{\tau}{2}\right) \mathrm{e}^{-\mathrm{j}2\pi\theta t} \, \mathrm{d}t. \tag{3}$$

If we take σ to be large, then the kernel approaches one and the Choi–Williams distribution approaches the Wigner distribution. For small values of σ, the effect of the multiplication is to preserve the ambiguity function close to the axes of the θ, τ plane while attenuating the components apart from the axes. Since in multi-component signals the authentic terms are generally close to the axes of the ambiguity plane while the interference terms are scattered away from them, the resulting characteristic function may suppress the interference terms without markedly affecting the signal components.

3. ARMAV TECHNIQUE

For a linear multi-degree-of-freedom (m.d.o.f.) mechanical system with a second order differential equation

$$\mathbf{M}\ddot{\mathbf{X}} + \mathbf{C}\dot{\mathbf{X}} + \mathbf{K}\mathbf{X} = \boldsymbol{\eta}(t), \tag{4}$$

where $\mathbf{M}$, $\mathbf{C}$ and $\mathbf{K}$ are the system mass, damping and stiffness matrices ($n \times n$), respectively, $\mathbf{X}$ is the ($n \times 1$) vector of displacement responses and $\eta(t)$ is the ($n \times 1$) unmeasured excitation vector. The observation equation is given by

$$\mathbf{Y} = \mathbf{L}\mathbf{X}, \tag{5}$$

where $\mathbf{Y}$ is the ($m \times 1$) output observation vector, and matrix $\mathbf{L}(m \times n)$ specifies which d.o.f.s of the system are observed.

The modal characteristics of this system μ and the modal shapes or eigenvectors φ_μ are the solutions of the following equations:

$$(\mathbf{M}\mu^2 + \mathbf{C}\mu + \mathbf{K})\boldsymbol{\psi}_\mu = 0, \qquad \varphi_\mu = \mathbf{L}\boldsymbol{\psi}_\mu. \tag{6, 7}$$

The state-space model of this mechanical system can be given by equations (8) and (9):

$$\dot{\mathbf{Z}} = \mathbf{A}\mathbf{Z} + \mathbf{B}\boldsymbol{\eta}(t), \qquad \mathbf{Y} = \mathbf{H}\mathbf{Z}, \tag{8, 9}$$

where $\mathbf{Z}$ is the $2n$-dimensional state vector, defined as

$$\mathbf{Z} = \begin{Bmatrix} \mathbf{X} \\ \dot{\mathbf{X}} \end{Bmatrix} \tag{10}$$

and $\mathbf{A}$, $\mathbf{B}$, $\mathbf{H}$ are ($2n \times 2n$), ($2n \times n$), ($m \times 2n$) matrices, respectively,

$$A = \begin{bmatrix} \mathbf{0} & \mathbf{I} \\ -\mathbf{M}^{-1}\mathbf{K} & -\mathbf{M}^{-1}\mathbf{C} \end{bmatrix}, \qquad \mathbf{B} = \begin{bmatrix} \mathbf{0} \\ \mathbf{M}^{-1} \end{bmatrix}, \qquad \mathbf{H} = [\mathbf{L}\ \mathbf{0}]. \tag{11}$$

After sampling with frequency f and transformation of the $2n$ first order differential equations (8) into a discrete-time equation, we obtain the following discrete-time state-space model and the discrete-time observation equation [15]:

$$z_{k+1} = \mathbf{F}z_k + v_k, \qquad y_k = Hz_k, \tag{12, 13}$$

where v_k represents the unobserved state vector of dimension $2n$; $\mathbf{F} = \mathrm{e}^{A/f}$ is the $(2n \times 2n)$ discrete-time state-space matrix or discrete-time transition matrix and v_k is given by

$$v_k = \int_0^{1/f} \mathrm{e}^{As}\mathbf{B}\eta(s)\,\mathrm{d}s. \tag{14}$$

The state-space innovation model in equation (12) and observation equation (13) constitute a suitable representation for the synthesis of regularly sampled randomly excited vibrating systems. The modal characteristics defined in equations (6) and (7) can be equivalently found in the eigenstructure $(\lambda, \varphi_\lambda)$ of the transition matrix F:

$$\lambda = \mathrm{e}^{u/f}, \qquad \varphi_u = \mathbf{H}\varphi_\lambda. \tag{15}$$

Our objective is to find the modal parameters from multiple output data y_k only. At this part our interest is focused on the mixed vector (or multivariate) auto-regressive moving average representation for the $\{y_k\}$ process. For the m-dimension stationary processes y_k, the ARMAV (p, q) model can be represented as follows [16]:

$$\mathbf{Y}[n] = \sum_{k=1}^{p} \mathbf{A}[k]\mathbf{Y}[n-k] + \mathbf{U}[n] + \sum_{k=1}^{q} \mathbf{B}[k]\mathbf{U}[n-k], \tag{16}$$

where $\mathbf{Y}[n]$, $\mathbf{U}[n] \in \mathbf{R}^m$ and $\mathbf{A}[k] \in \mathbf{R}^{m,p}$, $\mathbf{B}[k] \in \mathbf{R}^{m,q}$.

The above model assumes that the output is a weighted average of the preceding q input terms—a moving average—and the previous p output terms—an auto-regressive average. Lutkepohl [17], Akaike [18] and Reinsel [19] had studied how to get the coefficients $\mathbf{A}[k]$ from y_k.

The companion matrix $\mathbf{B}$ $(mp \times mp)$ based on the coefficients $\mathbf{A}[k]$ can be obtained as follows:

$$\mathbf{B} = \begin{bmatrix} \mathbf{0} & \mathbf{I} & \cdots & & \\ \vdots & \vdots & \cdots & \vdots & \mathbf{0} \\ & \mathbf{0} & \cdots & \mathbf{I} & \\ & & \cdots & & \mathbf{I} \\ \mathbf{A}[1] & \mathbf{A}[2] & \cdots & \mathbf{A}[p-1] & \mathbf{A}[p] \end{bmatrix}. \tag{17}$$

From the companion matrix, the eigenvalues λ and the eigenvectors φ_λ can be obtained. So from equation (15), complex eigenvalues μ, defining the natural frequencies and modal damping factors, and the modal shapes φ_μ can also be acquired.

4. CASE STUDY

4.1. THE HUMAN BRIDGE MONITORING SYSTEM

The Humen bridge, a six-lane highway suspension bridge, lies at the Zhujiang Delta in Guangdong province, China, and spans the mouth of Zhujiang River. It has a main span of 888 m, and a total length of 15·762 km. This bridge has important structural features: the streamlined, low-drag, closed box-girder steel decks exhibit negative lift in wind conditions [20]. This means that the cross-section of the bridge is an inverted airfoil. Hence, as the

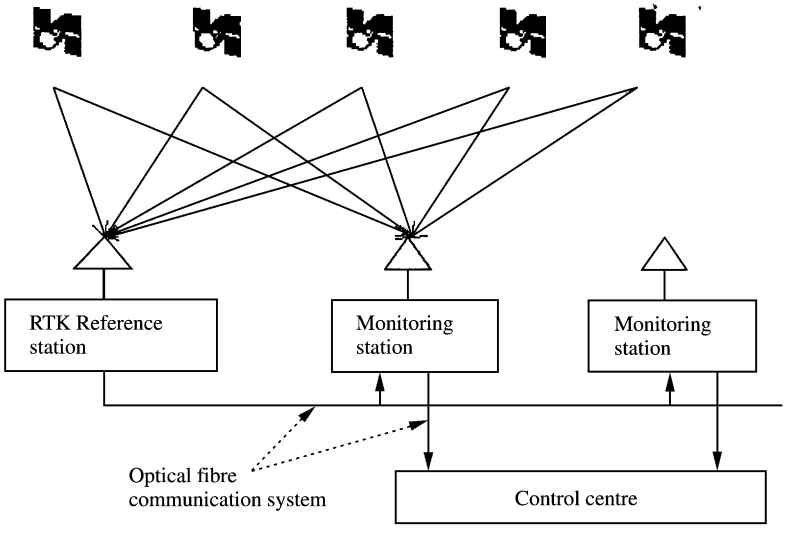

Figure 1. The Humen bridge on-line RTK-GPS monitoring system.

wind force increases, the bridge deck is forced downward as it is also twisted. The Humen bridge is located in a subtropical–tropical area, and is subject to strong typhoons every summer. On one occasion, tens of vehicles stopped on the central span of the bridge because drivers were too afraid to drive forward because of the high-amplitude vibration of the bridge in the strong wind.

For safety reasons, a global positioning system (GPS) monitoring system was designed and installed on the Humen bridge to provide long-term and real-time measurement of bridge movement. The Humen bridge monitoring system [21] consists of a real-time kinematic (RTK) reference station, a total of 12 GPS monitoring stations, an optical fibre communication system (instead of a radio communication system [22], in which signal loss may occur under certain circumstances) and a control centre. A detailed drawing of the system is shown in Figure 1.

The GPS reference station, equipped with a double-frequency GPS receiver, is located on the top of the building of the control centre whose 3-D coordinate had been previously determined by conventional static GPS methods. It is located in an open space away from the influence of radio stations, and within 300 m of the bridge. The reference station refreshes the RTK correction messages for the GPS monitoring stations with a frequency of 1 Hz via the optical fibre communication system. Twelve GPS monitoring stations were fixed to the main span of the bridge with 10 on both sides of the bridge deck (1/2, 1/4 and 1/8 spans) and two on the bridge towers (see Figure 2). The fixings did not allow any relative movement of the GPS monitoring stations and the bridge structure. (*Note*: in the first stage, only seven GPS monitoring stations were installed. These are numbered from 1 to 7 as shown in Figure 2).

An optical fibre communication network was installed to transmit RTK signals to avoid potential signal loss caused by large vehicles blocking GPS signal paths. The optical fibre communication network uses two-way transmission links between the control centre, reference station and the monitoring stations. The control centre consists of an operation server, several analysis workstations and an industrial communication PC that is used for communication between the control centre and GPS monitoring stations. The operation

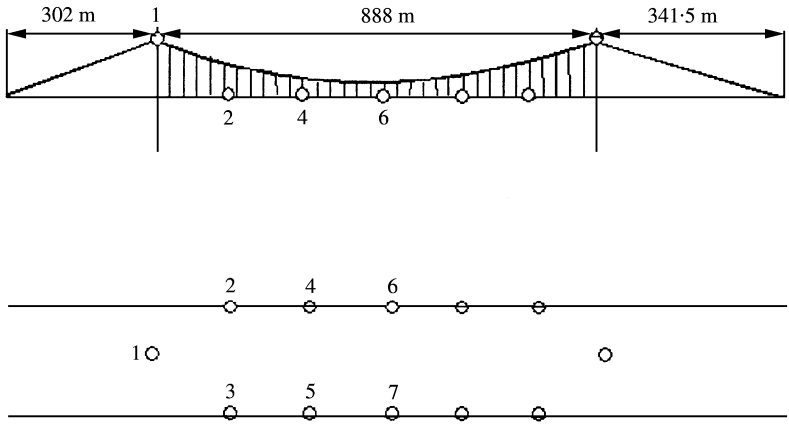

Figure 2. Locations of GPS monitoring stations on the bridge.

server is used for system control, administration and data processing. The analysis workstations are used for GPS monitoring, information analysis and graphic presentation.

The resolution (i.e., potential accuracy) of the RTK GPS technique over short distances and under low dynamics was determined through a zero-baseline test. The zero-baseline test consisted of two Dassoalt–Sercel dual-frequency GPS receivers attached to a single GPS antenna, receiving the same signals from the GPS satellites. The data collected were mixed with that generated by the receivers' own oscillators, and then processed using the Sercel RTK software. Because of the cancellation of many of the systematic errors, a zero-baseline test gives an indication of the resolutions of the measurement system, and hence of the accuracy which can ultimately be achievable. The results show that the system has a resolution of ± 5 mm horizontally and ± 10 mm in height.

This technique has several advantages: the monitoring stations can RTK orient only if they receive the difference signal from five or more GPS satellite and base station. As a result the data of these remote stations are synchronous and real time; the resolution of the changes in distance is 10 mm and the sampling rate is 5 Hz. The 3-D data can be passed to monitoring centre directly for safe analysis.

4.2. WIND-INDUCED VIBRATIONS

During the passage of a typhoon from 8 a.m. to 20 p.m. on 17 July 2000, field data of 12 h were recorded. The lateral, vertical and torsion time plots corresponding to the maximum wind speed are shown in Figures 3–5. Figure 6 shows the maximum wind speed time histories of the 20 min record with a sampling period of 2·5 min.

It can be seen that the peak vertical displacement at quarter-span is much larger than the displacement at the mid-span. But the peak torsional response at quarter-span is much smaller than the response at the mid-span. This phenomenon is probably due to the fact that the first vibration mode has the greatest contribution to structural response. For Humen bridge, the first vertical vibration mode shape is antisymmetrical and the first rotational vibration mode shape is symmetrical [23]. Therefore, the maximal vertical response occurs at quarter-span while the maximal rotational response occurs at mid-span [20].

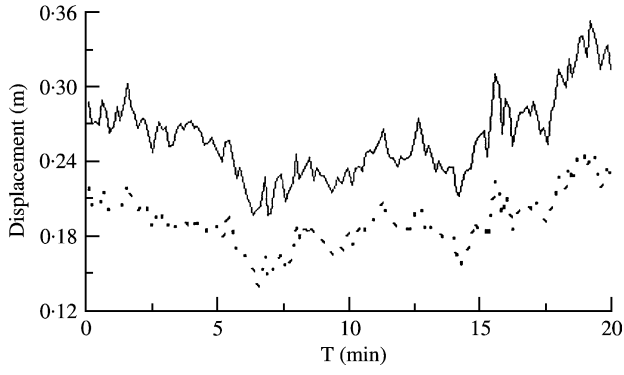

Figure 3. The wind-induced lateral displacement response of bridge. ——, half; – – – –, quarter.

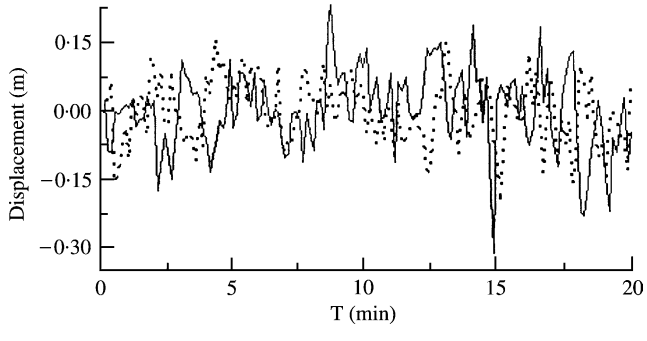

Figure 4. The wind-induced vertical displacement response of bridge. – – – –, half; ——, quarter.

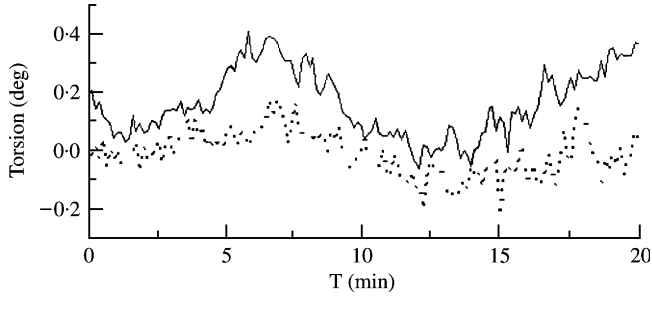

Figure 5. The wind-induced torsion displacement response of bridge. ——, half; – – – –, quarter.

5. SYSTEM IDENTIFICATION

5.1. PRE-PROCESSING

Pre-processing is the data treatment before system identification and the result highly influences the identification effect. The following possibilities are included:

Decimate: The data are low-pass filtered and decimated so that the identification can concentrate on a limited frequency band.

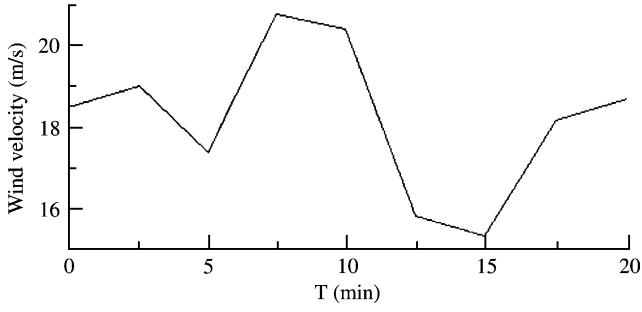

Figure 6. Time histories of wind speed.

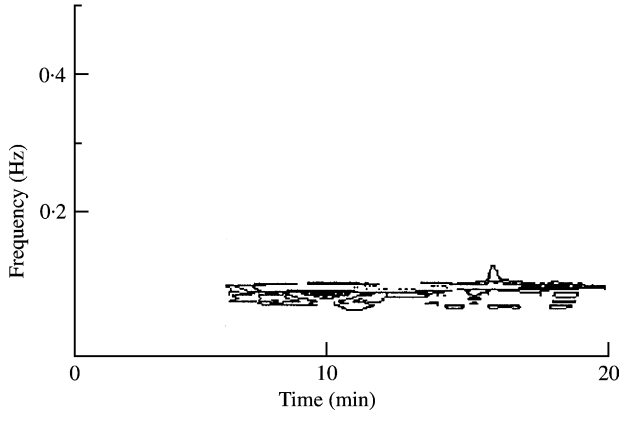

Figure 7. Scalogram of the displacement responses of the bridge in the lateral directions.

Detrend: The best straight-line fit is removed from the data. The treatment enables the removal of the DC-components that can badly influence the identification results.

De-noise: The useful information reflecting the structural condition is extract from the highly noised signal.

5.2. WD ANALYSIS

In the phase plane, formed by time and frequency, the frequencies can be displayed on a two-dimensional time–frequency plane that is called a scalogram. It is possible to identify the energy content of the signal at different frequencies when the time is given. This scalogram is different from the short-time FFT (STFT), because STFT is essentially applying FFT with a short moving time window repeatedly to a long time series to obtain its time–frequency representation. To represent the signal with more detail in the time domain, we have to make the time window smaller. If the sampling rate of the signal remains the same, the method of choosing a smaller time window makes the frequency resolution worse. So good resolutions both in the time and frequency domains cannot be achieved at the same time.

Figures 7–9 are the scalograms of the responses of the bridge in the lateral, vertical and torsion directions respectively. This scalogram gives energy content in the time–frequency

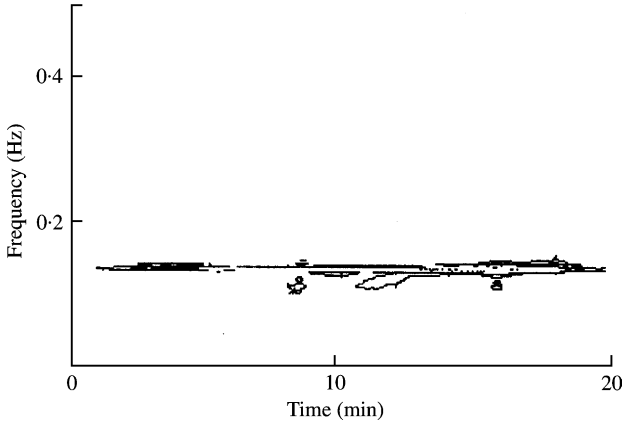

Figure 8. Scalogram of the displacement responses of the bridge in the vertical directions.

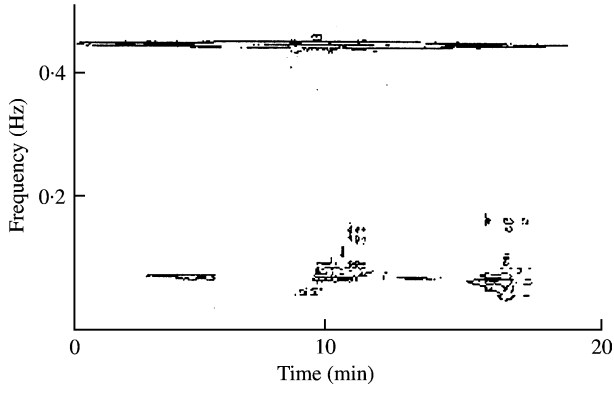

Figure 9. Scalogram of the torsion responses of the bridge.

domain, where the band indicates the relative contributions of different sway modes. It is clearly found that in these three scalograms, the overall lateral response of the bridge is dominated by frequency 0·095, which corresponds to the first lateral sway mode. At the same times the overall vertical response of the bridge is dominated by frequency 0·134, which corresponds to the first vertical sway mode. To the overall torsion response, the scalogram is dominated by frequency 0·446, which corresponds to the first torsion sway mode. But in torsion scalogram, the first lateral sway frequency 0·095 is also clear, which can be attributed to the coupling effect between the lateral and torsion.

It also can be seen in Figures 7–9 that the dark frequency is not uniform along the time axis and the non-stationary of the displacement response was verified. This illustrates the transient characteristics of the energy content along the time axis. Therefore, the WD brings out the transient characteristics of the wind-induced vibration of the bridge.

5.3. ARMAV AND FFT MODAL ANALYSIS

ARMAV time-domain modal analysis technique and FFT frequency modal analysis technique are also applied to extract the modal parameters of the Humen bridge in order to

TABLE 1

Comparison of the modal results

	ARMAV		FFT	
Mode	Freq. (Hz)	Damping (%)	Freq. (Hz)	Damping (%)
1	0·095	2·48	0·094	2·71
2	0·134	1·32	0·134	1·54
3	0·170	0·88	0·168	0·67
4	0·225	0·71	0·229	0·75
5	0·277	0·68	0·277	0·63
6	0·368	0·52	0·365	0·43
7	0·447	0·44	0·442	0·35

compare the three different modal identification techniques. Part three shows the ARMAV modal identification process, as for the FFT, the natural frequencies are simply determined by picking the peaks on the graphs of the averaged normalized power spectral densities (ANPSD), which are basically obtained by FFT. The components of the mode shapes are determined by the values of the transfer functions at the natural frequencies. Transfer functions are defined as follows:

$$\frac{\phi_{ki}}{\phi_{pi}} = \frac{S_{pk}(\omega_i)}{S_{pp}(\omega_i)}, \tag{18}$$

where ϕ_{ki}, ϕ_{pi} are the GPS monitoring station (k, p) ith model shapes values, S_{pk} is the cross power spectral densities of GPS monitoring station (k, p) and S_{pp} is the power spectral densities of GPS monitoring station p. The results are show in Table 1.

Totally, seven modes were extracted by these two methods. The frequencies of the seven modes are less than 0·5 Hz, much lower than the GPS sampling rate, implying that no severe frequencies confusion can occur. The damping ratios obtained from the experiments methods are usually lower than 1%, validating that under elastic small displacement, the damping ratios of steel suspension bridge are really low [24].

6. CONCLUSIONS

Three signal analysis techniques were applied to obtain modal parameters from the same wind-induced response. All the three methods can identify the first lateral, vertical and torsion modes. The WD technique, as a time–frequency approaching structural identification, has the following three advantages. Firstly, a close modal coupling can be recognized due to the different energy content ratio of coupled modes along the time axis. Secondly, non-stationary can be revealed by the scalograms. Finally, the frequency peak values deviate from constant value along the time axis when non-stationary displacement responses arise. From the scalograms the frequency change with the wind speed can also be observed. This technique seems to be the best for quantitative study of fast-changing transient signals.

The FFT technique is a frequency-domain approach to structural identification. This identification process is so fast that it can be used on site to verify the quality of the measurements. But its frequency resolution is low and damping estimates are unreliable.

Time-domain analysis based on ARMAV models allows for gaining high-frequency resolution. But it is strictly related to the stationary hypothesis.

It is a general conclusion that these three techniques will improve the quality of the analysis by providing more aspects to look at the characteristics of the signal. FFT technique can be used for on-line health monitoring, while the WD combined with ARMAV seems to be the best case in quantitative analysis of fast-changing vibration signals.

REFERENCES

1. S. R. IBRAHIM and E. C. MIKULCIK 1973 *The Shock and Vibration Bulletin* **43**, 21–37. A time domain modal vibration test technique.
2. H. A. COLE 1968 *AIAA Paper No.* 68-288. On-the-line analysis of random vibrations.
3. H. A. COLE 1973 *NASA CR*-2205. On-line failure detection and damping measurement of aerospace structures by random decrement signatures.
4. C. S. HUANG 1999 *Earthquake Engineering and Structural Dynamics* **28**, 857–878. Dynamic testing and system identification of a multi-span highway bridge.
5. S. M. PANDIT and N. P. METHA 1985 *Journal of Dynamic Systems, Measurement, and Control* **107**, 132–138. Data dependent system approach to modal analysis via state space.
6. B. PIOMBO, E. GIORCELLI, L. GARIBALDI and A. FASANA 1992 *Proceedings of the* 17*th International Seminar on Modal Analysis, Leuven*, Vol. 2, 721–732. ARMAV approach for large structure identification.
7. L. GARIBALDI, E. GIORCELLI and B. PIOMBO 1998 *Journal of Vibration and Acoustics* **120**, 713–718. ARMAV techniques for traffic excited bridges.
8. B. PEETERS and G. DE ROECK 1999 *Proceedings of the* 2*nd International Conference on Identification in Engineering Systems, Swansea, U.K.* 639–648. Based stochastic subspace identification in civil engineering.
9. J. Q. FANG, Q. S. LI and D. K. LIU 2000 *Proceedings of the Institution of Civil Engineers, Structures and Buildings* **140**, 151–159. Wind effects on a very tall building and vavelet analysis.
10. T. J. WAHL and J. S. BOLTON 1993 *Journal of Sound and Vibration* **163**, 101–122. The application of the Wigner–Ville distribution to the identification of structure-borne noise components.
11. N. YEN 1987 *Journal of Acoustical Society of America* **81**, 1841–1850. Time and frequency representation of acoustic signals by means of the Wigner distribution function: implementation and interpretation.
12. P. BONATO and R. CERAVOLO 1998 *Journal of Wind Engineering and Industrial Aerodynamics* **74–76**, 709–718. The use of wind excitation in structural identification.
13. F. HLAWATSCH and G. F. BOUDREAUX-BARTELS 1992 *IEEE Signal Processing Magazine* **9**, 21–67. Linear and quadratic time–frequency signal representations.
14. H. I. CHOI and W. J. WILLIAMS 1989 *IEEE Transactions on Acoustics, Speech, and Signal Processing* **37**, 862–871. Improved time–frequency representation of multi-component signals using exponential kernels.
15. W. GERSCH and R. S. LIU 1976 *Journal of Applied Mechanics* **98**, 59–165. Time series methods for the synthesis of random vibration systems.
16. M. PREVOSTO and M. OLAGNON. 1991 *Journal of Sound and Vibration* **148**, 329–342. State space formulation: a solution to modal parameter estimation.
17. H. LUTKEPOHL 1993 *Introduction to Multiple Time Series Analysis.* Berlin: Springer-Verlag.
18. H. AKAIKE 1973 *Biometrika* **60**, 255–265. Maximum likelihood identification of Gaussian autoregressive moving average models.
19. G. C. REINSEL 1993 *Elements of Multivariate Time Series Analysis.* Berlin: Springer-Verlag.
20. Y. DACHUN and H. YIANYU 1995 *China Journal of Highway and Transport* **8**, 63–70. A study of static characteristics of girder section of Humen suspension bridge by aerodynamic tests.

21. X. LIANG, G. JINJUN and D. LIANJUN 2001 *Geotechnical Investigation and Surveying*, *Beijing*, Vol. 165, 47–49. The data analysis to real time displacement of Humen Bridge by GPS.
22. C. J. BROWN, R. KARUNA, V. ASHKENAZI, G. W. ROBERTS and R. A. EVANS 1999 *Proceeding of The Institution of Civil Engineers*, *Structures and Building* **134**, 97–105. Monitoring of structures using the global positioning system.
23. Z. GUANGYONG and Z. LEDONG 1999 *Journal of Tongji University* **27**, 193–197. Test on vibration characteristics of Humen Bridge.
24. A. M. ABDEL-GHAFFAR and R. H. SCANLAN 1985 *Journal of Engineering Mechanics*, *American Society of Civil Engineers* **111**(4), 463–499. Ambient vibration studies of Golden Gate Bridge: I & II.